CO2 and CH4 Separation by Adsorption Using Cu-BTC Metal–Organic Framework
— Source link ↗

Lomig Hamon, Elsa Jolimaitre, Gerhard D. Pirngruber

Related papers:

- Selective gas adsorption and separation in metal–organic frameworks

- A chemically functionalizable nanoporous material (Cu3(TMA)2(H2O)3)n

- Metal-organic frameworks with exceptionally high capacity for storage of carbon dioxide at room-temperature

- CO2 Adsorption-Based Separation by Metal Organic Framework (Cu-BTC) versus Zeolite (13X)

- Carbon Dioxide Capture in Metal–Organic Frameworks

CO 2 and CH 4 Separation by Adsorption Using Cu-BTC Metal-Organic Framework

Lomig Hamon, Elsa Jolimaître, Gerhard D. Pirngruber

CO$_2$ and CH$_4$ Separation by Adsorption Using Cu-BTC Metal−Organic Framework

Lomig Hamon, Elsa Jolimaître, and Gerhard D. Pirngruber*

IFP-Lyon, Catalysis and Separation Division, Rond-Point de l'Échangeur de Solaize, 69360 Solaize, France

Molecular simulations have shown that the metal−organic framework Cu-BTC (Cu$_3$(BTC)$_2$) is an interesting candidate for the separation of CO$_2$ by adsorption. In this work, the first experimental binary and ternary adsorption data of CO$_2$, CH$_4$, and CO on the Cu-BTC are reported. These data are analyzed and compared with coadsorption models that are built from pure component isotherm data. Cu-BTC has a CO$_2$/CH$_4$ selectivity of ~8 and a high delta loading (=difference between adsorption capacity under conditions of adsorption and desorption) and therefore appears to be a good compromise between zeolites, with high selectivity for CO$_2$, but low delta loadings, and activated carbons, with high delta loadings, but low selectivity, for pressure swing adsorption applications.

Introduction

Hydrogen is mainly produced by steam reforming of natural gas, a process which generates a synthesis gas mixture containing H$_2$, CO$_2$, CO, and CH$_4$ (and eventually some other impurities). Pure H$_2$ is obtained from this synthesis gas mixture by pressure swing adsorption (PSA). A series of different adsorbents remove the impurities (CO$_2$, CO, and CH$_4$), and H$_2$ of very high purity leaves the adsorber column at high pressure. The adsorbed impurities are then recovered from the column by desorption during a low-pressure purge (which explains the name pressure swing). The CO$_2$−CH$_4$−CO purge gas is normally used as combustible for the steam reformer, but in view of the current concerns about CO$_2$ emissions this is not the ideal solution. Methods would be needed to produce a separate waste stream of pure CO$_2$, which could then be sequestered, and recycle only CH$_4$ and CO as fuels to the steam reformer. For that purpose, adsorbents have to be developed that selectively adsorb CO$_2$, i.e., that separate CO$_2$ from CO and CH$_4$.

CO$_2$ selective adsorbents are also needed in the purification of biogas, which is essentially a mixture of CO$_2$ and CH$_4$. The objective is to produce pure CH$_4$ as a fuel and to lose as little CH$_4$ as possible in the CO$_2$ waste stream.

Recently metal−organic frameworks (MOFs) have attracted attention as adsorbents for the separation of CO$_2$ and CH$_4$.[1–4] These new microporous materials, which are formed by the combination of metallic clusters with organic ligands, present high adsorption capacities and could potentially be used for the separation of CO$_2$, CH$_4$, and CO.[5,6] In this study, we focus on the Cu$_3$(BTC)$_2$ or Cu-BTC or HKUST-1.[7] This MOF is easily synthesized from nonexpensive primary compounds and is also commercially available. This microporous material is made of copper clusters linked to each other via trimesic acid (Figure 1). It forms a structure presenting a large pore surrounded by eight small pores called side pockets. The window between large pore and side pocket exhibits a triangular shape limited by trimesic acid with a window size of 4.6 Å. Recent papers compared the experimental adsorption of pure CH$_4$[8–10] and pure CO$_2$,[8,11–17] and several studies presented molecular simulations of the adsorption of the CO$_2$−CH$_4$ binary mixtures, predicting

a high selectivity of Cu-BTC for CO$_2$.[9,18–22] Surprisingly, no experimental data of the mixture adsorption are yet available, but such data are needed if we want to develop new adsorption processes based on Cu-BTC.

In this paper, we therefore focus on coadsorption measurements of binary and ternary mixtures of CO$_2$, CH$_4$, and CO on Cu-BTC. The experimental coadsorption results are compared to predictions from coadsorption models that rely on pure component isotherms only. Finally, we compare the performance of Cu-BTC in the separation of synthesis gas mixtures by PSA to conventional adsorbents, i.e., activated carbons and zeolite Na−X.

Experimental Section

Synthesis. Cu-BTC has been synthesized according to the modus operandi of Bordiga et al.[23] A 30.51 g amount of CuNO$_3$·3H$_2$O was dissolved in a 500 mL 50/50 (v/v) water−ethanol mixture. After adding 17.84 g of trimesic acid, the solution was filled in a 1 L Teflon liner placed in an autoclave. It was heated to 393 K for 24 h and then filtered and washed with ethanol.

Characterization. A Brunaer−Emmett−Teller (BET) surface area determination was carried out using a Micromeritics ASAP 2000 instrument. Before measurement, the sample was outgassed under secondary vacuum at 423 K overnight. X-ray diffraction (XRD) patterns were recorded with a Bruker AXS D4 Endeavor diffractometer (2θ values between 2 and 60° with a step of 60 s; 1 step, 0.02°; Cu Kα radiation with a wavelength of 1.5406 Å) on a dried sample of Cu-BTC as powder. Thermogravimetric (TG) analysis was carried out with a Netzsch TG 209 F1 apparatus under a helium atmosphere at 100 kPa controlled by a flow meter with a flow rate of 3 NL·h^{-1}. A first measurement was performed from 296 K up to 773 K with a temperature rate of 5 K·min^{-1} to record a complete TG analysis. In the aim to check the thermal stability of the Cu-BTC sample, a second TG analysis was recorded, cycling the temperature with a rate of 3 K·min^{-1} from 298 to 473 K, and a 15 min hold; cycles were repeated 5 times.

Gravimetric Measurements. Pure CO$_2$, CH$_4$, and CO adsorption measurements were carried out using a high-pressure magnetic suspension balance marketed by Rubotherm (Rubotherm Präzisionsmesstechnik GmbH).[24,25] Approximately 1 g of sample was used for the experiments. The material was

* To whom correspondence should be addressed. E-mail: gerhard.pirngruber@ifp.fr. Tel.: +33 478 022 733. Fax: +33 478 022 066.
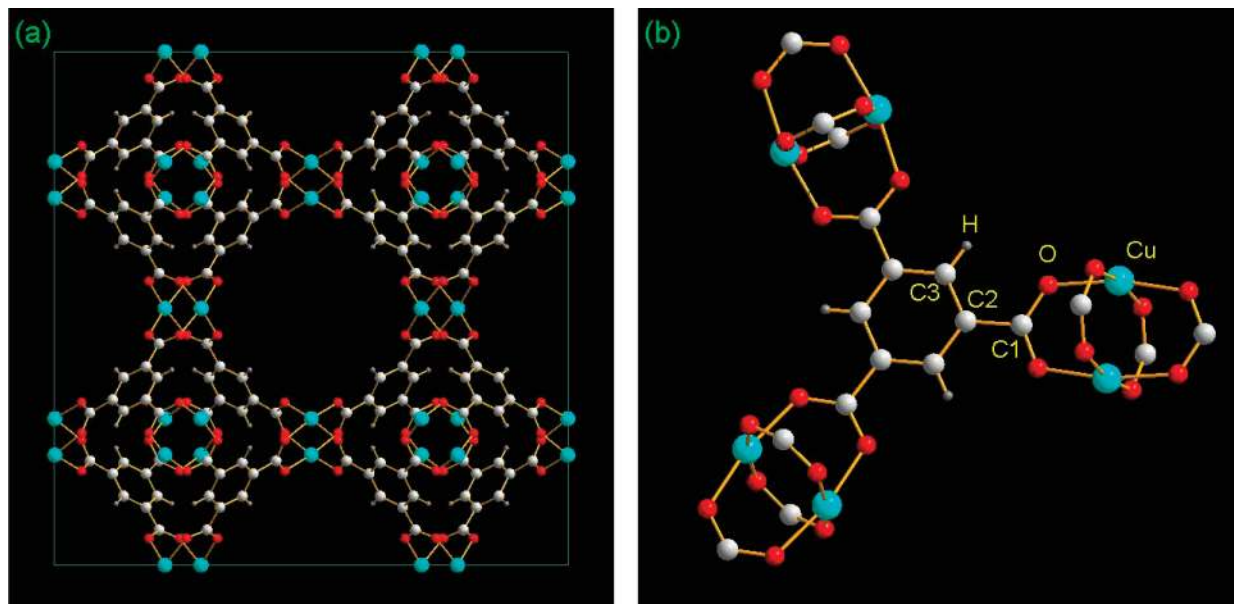
Figure 1. (a) Unit cell crystal structure of the Cu-BTC along the [100] direction. (b) Cluster of the Cu-BTC. (Cu, green; O, red; C, white; H, gray).

activated and outgassed between each experiment under secondary vacuum at 448 K with a temperature ramp of 1 K·min^{-1}. The buoyancy effect of the gas phase on the adsorbent volume and on the volume of the adsorbed phase, which is supposed to be equal to the micropore volume of the solid, is corrected for, so as to determine the absolute adsorbed mass.[26] We prefer here to work with absolute adsorbed amounts instead of excess adsorbed amounts, to facilitate the comparison with the results of breakthrough experiments. The gas density is determined using an appropriate equation of state (EoS).[27,28] The adsorbent volume is evaluated by measuring the buoyancy effect of helium, supposing that helium does not adsorb. Helium density is determined using a modified Benedict−Webb−Rubin EoS.[29]

Breakthrough Curve Measurements. CO_2−CH_4 binary and CO_2−CH_4−CO ternary mixture adsorption measurements were carried out using a homemade breakthrough curve apparatus, allowing one to perform measurements from atmospheric pressure up to 5.0 MPa (see the Supporting Information for more details). Gas mixtures were generated in situ. The sample (2.89 g) was packed into the column as powder (not pelletized) and was activated and outgassed at 448 K (rate of 1 K·min^{-1}) under a helium flow of 1 N·L·h^{-1}. Breakthrough curve measurements were carried out in two steps: The feed gas mixture (total gas flow rate is 4 N·L·h^{-1}) is first injected in the column, which is under helium atmosphere at the pressure of the experiment. This method allows one to evaluate the adsorbed amount of CO_2, but uncertainties on the determination of CH_4 are large due to the roll-up effect (vide infra). Therefore, a second experiment is carried out. The CO_2−CH_4 mixture is injected on a CO_2-presaturated column at the pressure of the experiment. This method yields a CH_4 breakthrough curve without roll-up and, thus, reduces the uncertainty of the evaluation of the first moment of the CH_4 breakthrough curve. The breakthrough experiments were carried out between 0.1 and 1.0 MPa. The pressure drop over the column was always less than 0.005 MPa.

The (absolute) adsorbed amount is calculated from the first moment of the breakthrough curve (after correction for the dead time) by the equation

$$q_i = \frac{C_i}{m_{ads}}\left(Q\mu - V_{col} + \frac{m_{ads}}{\rho_{grain}}\right) \qquad (1)$$

The selectivity is calculated as

$$S_{1,2} = \frac{q_1/y_1}{q_2/y_2} \qquad (2)$$

where q_i is the adsorbed amount of compound i and y_i is the mole fraction of compound i in the gas phase. On the basis of reproducibility measurements as well as theoretical calculations of the error margin, we estimate that the error of our selectivity values is approximately 20%.

Breakthrough Curves Model. The main assumptions of the model are as follows: (1) The flow pattern is described by the axially dispersed plug-flow model. (2) The column is isothermal. (3) Frictional pressure drop through the column is negligible. (4) The variation of fluid velocity along the column length, as determined by the global mass balance, is accounted for. (5) An external film resistance between the fluid and the crystal surface is assumed (in practice, this resistance was found to be negligible in our experimental conditions; it was nevertheless kept in the model, for numerical considerations). (6) Diffusion in the crystal follows Fick's law. The driving force is the gradient of adsorbed phase concentration, and the diffusion coefficient is constant. Using the above hypotheses, a set of well-known equations can be established (see Table 1).

Equations were written in the collocation form, thus reducing the set of partial differential equations to a set of algebraic and ordinary differential equations. These equations were then numerically integrated using the IMSL DASPG routine, based on Petzold−Gear's integration method.

Results

Characterization of the Materials. The XRD pattern of our Cu-BTC sample is similar to the theoretical one. The material was stable up to 500 K. The N_2 isotherm at 77 K exhibits a kink, which can be attributed to the presence of the side pockets and the large pores.[30−33] The BET surface area is 2211 m^2·g^{-1}, and the micropore volume is 0.813 cm^3·g^{-1} (see the Supporting Information for more details).

Single Component Adsorption Measurements. Adsorption isotherms of pure CO_2, CO, and CH_4 have type I shapes (see Figure 2) according to the IUPAC classification.[34] A hysteresis

Table 1. Equations of the Breakthrough Curve Model

fluid phase	$\dfrac{\partial C_i}{\partial t} = D_L \dfrac{\partial^2 C_i}{\partial z^2} - \dfrac{\partial v C_i}{\partial z} -$ $\left(\dfrac{1-\varepsilon_i}{\varepsilon_i}\right)\dfrac{3}{R_c}k_t(n_i^* - n_i\vert_{r=R_c})$
	$\dfrac{\partial v C_i}{\partial z} = v\dfrac{\partial C_i}{\partial z} + C_i\dfrac{\partial v}{\partial z}$
	$\dfrac{\partial C_i}{\partial z}\bigg\vert_{z=L} = 0$
	$D_L\dfrac{\partial C_i}{\partial z}\bigg\vert_{z=0} = -v_0(C_i\vert_{z=0-} - C_i\vert_{z=0+})$
velocity variation	$C_T\dfrac{\partial v}{\partial z} = -\dfrac{1-\varepsilon_i}{\varepsilon_i}\dfrac{3k_t}{R_c}\sum\limits_{j=1}^{N}(n_i^* - n_j\vert_{r=R_c})$
crystal	$\dfrac{\partial n_i}{\partial t} = \dfrac{D_c}{r^2}\dfrac{\partial}{\partial r}\left(r^2\dfrac{\partial n_i}{\partial r}\right)$
	$\dfrac{\partial n_i}{\partial r}\bigg\vert_{r=0} = 0$
	$D_c\dfrac{\partial n_i}{\partial r}\bigg\vert_{r=R_c} = k_t(n_i^* - n_i\vert_{r=R_c})$
thermodynamic equilibrium conditions	$n_i^* = n_{i,\text{sat.}}\dfrac{B_iC_i\vert}{1+\sum\limits_j B_jC_j}$

is not observed. The maximum adsorbed quantity of CO_2 is 14 mmol·g^{-1} (135 molecules·(unit cell)$^{-1}$), CO, and CH_4 did not reach saturation in our measurements. The CO_2 isotherm is similar to those already measured by several authors,[8,11,14,16] except for Cu-BTC prepared in a mixture of water−ethanol− DMF (DMF = dimethylformamide)[11] or prepared in a water−ethanol mixture but washed with methanol.[16] It is well-known that it is difficult to remove DMF entirely from the pores of Cu-BTC, which results in a reduced adsorption capacity.[35] Our results for the adsorption of CH_4 are also similar to previous measurements[8,15] except for Cavenati et al.[14] who obtained smaller adsorbed quantities on a pelletized sample.
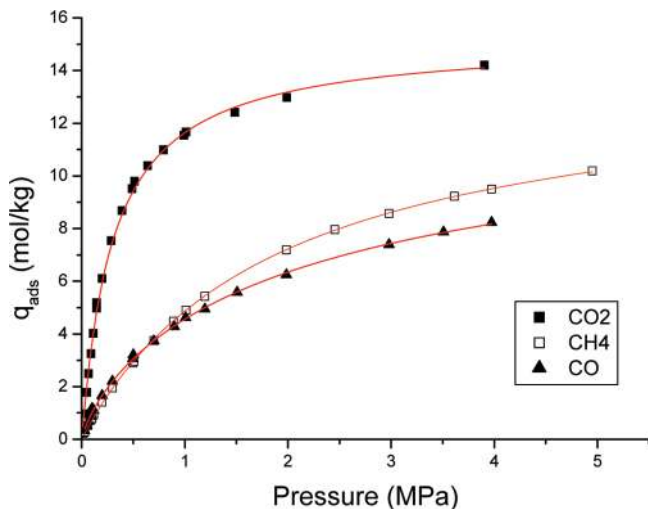

Figure 2. Absolute adsorbed amounts of pure CO_2 (full squares), CH_4 (open squares), and CO (triangles) at 303 K and the corresponding Langmuir (for CO_2 and CH_4) and Langmuir−Freundlich fits (for CO).

Table 2. Parameters of the Langmuir and Langmuir−Freundlich Isotherms That Fit Best the Experimental Isotherms of Pure CO_2, CO, and CH_4 at 303 K

	CO_2 Langmuir	CH_4 Langmuir	CO Langmuir	CO Langmuir−Freundlich
$q_{\text{sat.}}$ (mmol·g^{-1})	15.21	14.00	10.44	13.45
b (MPa^{-1})	3.25	0.533	0.818	0.512
ξ	1	1	1	0.801

In analogy to the N_2 isotherm at 77 K, we would have expected to find a step or a kink in the isotherms of CO_2 and CH_4, due to the presence of two types of pores, i.e., the side pockets and the large pores. In practice such a kink cannot be distinguished in isotherms of Figure 2. When fitting the isotherms with a dual-site Langmuir model, using a minimization of the square residual, the fit converges to the equal values of the affinity coefficients of the two sites, i.e., to a single-site Langmuir isotherm. Hence, from a macroscopic point of view, the two types of pores are not sufficiently different to be distinguishable as two separate adsorption sites in the isotherms. Table 2 compiles the parameters of the Langmuir and Langmuir−Freundlich isotherms that fit best the experimental values. The Langmuir−Freundlich model allows one to fit the CO isotherm slightly better than a simple Langmuir equation.

Binary Mixture Adsorption. Breakthrough curve experiments were carried out at 303 K to evaluate the separation performance of the Cu-BTC. Three mixtures (25−75, 50−50, and 75−25 CO_2−CH_4) were tested at three pressures (0.1, 0.5, and 1.0 MPa). Figure 3 shows the breakthrough curves of the three mixtures at 0.5 MPa (the complete set of breakthrough curves is given in the Supporting Information). For all of the mixtures, CH_4 breaks first, testifying that it adsorbs least. For the first mixture, i.e., 25−75 CO_2−CH_4, the breakthrough curve of CH_4 exhibits a double roll-up. The first part of the roll-up corresponds to the partial desorption of CH_4 due to the adsorption of CO_2 (the CH_4 flow rate temporarily exceeds the feed flow rate). An additional peak is observed just before CO_2 breaks through the column: this peak is attributed to a temperature wave that accompanies (slightly runs ahead of) the concentration front of CO_2, due to the exothermic adsorption of CO_2. This temperature wave causes a rapid desorption of CH_4. The higher the concentration of CO_2 in the feed, the more this thermal effect becomes mixed with the classical roll-up (in particular for the 75−25 CO_2−CH_4 mixture).

The roll-up increases the uncertainty in the determination of the first moment of the CH_4 breakthrough curve. To determine the adsorbed quantity of CH_4 more precisely, a second experiment is carried out: the Cu-BTC sample is initially saturated under CO_2 atmosphere at the pressure of the experiment, and the CO_2−CH_4 mixture is then injected. In this case, the breakthrough curve of CH_4 has a classical shape; i.e., the roll-up is avoided (Figure 3d), but since there are no hysteresis effects, the adsorbed amount of CH_4 at the end of the experiment is the same as in the direct breakthrough (He → CO_2/CH_4).

Figure 4a shows the adsorbed amount of CH_4 and CO_2 for the equimolar mixture as a function of pressure (see the Supporting Information for other compositions). The CO_2−CH_4 selectivity (Figure 4b) is between 4.8 and 11.5 and has the tendency to increase at higher pressure but does not depend much on the composition of the gas mixture. The deviating values for the 75−25 CO_2−CH_4 mixture can be attributed to the higher uncertainty of the results when the mixture is poor in CH_4. Cu-BTC is less selective than zeolite Na−X or Na−Y
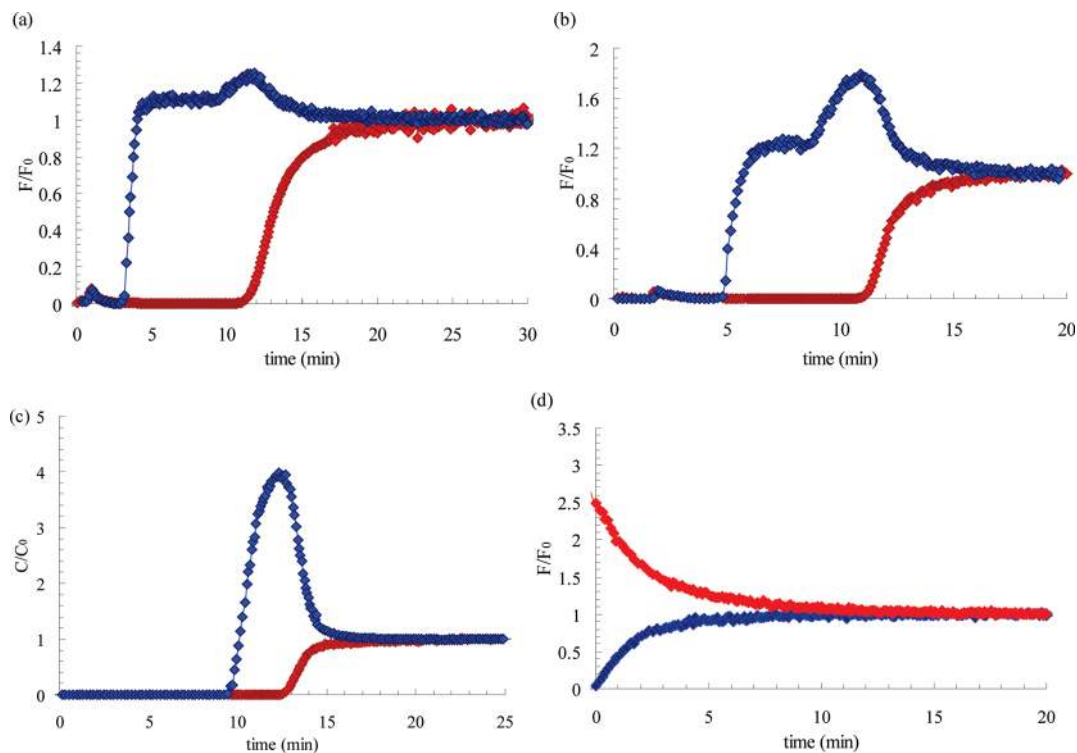
Figure 3. Breakthrough curve of CO_2 (red) and CH_4 (blue) at 0.5 MPa and 303 K for the 25−75 CO_2−CH_4 mixture (a), 50−50 mixture (b), and the 75−25 mixture (c) and the 50−50 mixture on a column presaturated with CO_2 (d).
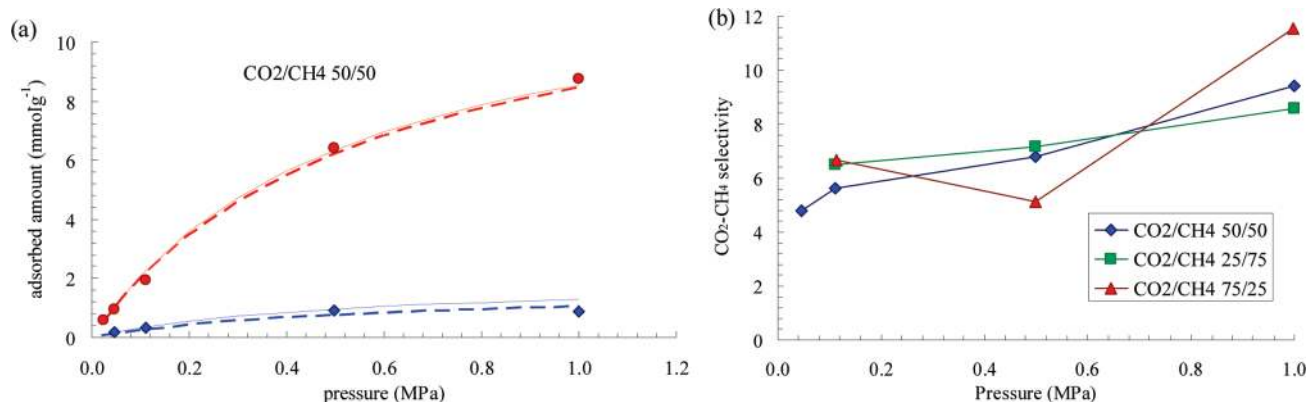

Figure 4. (a) Co-adsorption isotherm of the equimolar mixture of CO_2 (circles) and CH_4 (diamonds) at 303 K. Full lines represent the Langmuir model based on single-component isotherms; dashed thick lines, ideal adsorbed solution theory (IAST); dashed thin lines, the Langmuir model based on binary breakthrough experiments. (b) CO_2−CH_4 selectivity as a function of pressure for the three gas mixtures.

in the same experimental conditions[36] but significantly more selective than activated carbons.[37]

We wanted to verify whether it is possible to predict the coadsorption of CO_2 and CH_4 from the single-component isotherms, using either a simple multicomponent Langmuir model (eq 3) or ideal adsorbed solution theory (IAST).[38]

$$q_i = q_{i,\text{sat.}} \frac{b_i y_i}{1/p + b_{CO_2} y_{CO_2} + b_{CH_4} y_{CH_4}} \quad (3)$$

Figure 4 shows the coadsorption data calculated from eq 3 using the b and $q_{\text{sat.}}$ values of Table 1 (full lines). The selectivity in the Langmuir model is constant ($S = b_{CO_2} q_{\text{sat.}CO_2}/(b_{CH_4} q_{\text{sat.}CH_4})$ = 6.6). Hence, the Langmuir model does not describe the small increase in selectivity with pressure that was observed experimentally. It therefore slightly underestimates the adsorbed amount of CO_2 at high pressure and overestimates CH_4. When using IAST, the selectivity slightly increases with pressure (from

6.6 to 7.0), but the improvement is not significant. We have also observed that the IAST calculations are quite sensitive to the isotherm model that is used. For example, replacing a Langmuir isotherm by a Langmuir−Freundlich isotherm hardly changes the quality of the fit of the experimental pure component CO_2 isotherm but leads to a much stronger evolution of selectivity with pressure in IAST. For the use in breakthrough curve or PSA simulations, IAST also has the disadvantage of strongly increasing the computation time compared to the Langmuir model (eq 3).

We therefore thought that the best match with the breakthrough results would be obtained by fitting the Langmuir eq 3 with our coadsorption data (nine points, i.e., three compositions at three pressures). The new parameters are given in Table 3. The average selectivity is now 8.1. The quality of the fit of the experimental data hardly changes for CO_2 but improves for CH_4 at high pressure (dashed line in Figure 4).

Table 3. Single-Site Langmuir Parameters Obtained by Fitting the Binary CO_2–CH_4 Mixture Experimental Data

	CO_2	CH_4
$q_{sat.}$ (mmol·g^{-1})	15.67	10.18
b (MPa^{-1})	3.02	0.577

Breakthrough Curve Simulations. The input parameters of the model are listed in Table S1 and Table S2 of the Supporting Information. The axial dispersion coefficient is calculated from well-known correlations.[39] We compare two coadsorption Langmuir isotherms (eq 3), based on the parameters of Tables 2 and 3, respectively, i.e., either based on the pure component isotherms or on the coadsorption data. The only unknown parameters are the values of the diffusion coefficients of CO_2 and CH_4. For comparison with other MOFs, the CO_2 diffusion coefficient has been estimated (by uptake measurements) to be 7.9×10^{-13} and 1.72×10^{-8} m²·s^{-1} for the MOF-5,[40,41] and QENS yields a value of 10^{-8} m²·s^{-1} for the MIL-47(V).[42] The range of diffusion coefficients of CO_2 in zeolite Na–X is between 6.49×10^{15} and 3.4×10^{-10} m²·s^{-1}, depending on the measurement methods.[43–49] The discrepancies between these values have already been discussed by Kärger and Ruthven.[50] We chose, quite arbitrarily, an intermediate value of 1×10^{-10} m²·s^{-1} for both CO_2 and CH_4.

Figure 5 compares the simulated breakthrough curve obtained with the two coadsorption isotherms with the experimental curve. None of the two simulations fits the experimental curve of CO_2 well, because both isotherm models overestimate the equilibrium adsorption capacity by at least 10%. We have varied the isotherm parameters and the diffusion coefficients and have observed that the steepness of the breakthrough curve depends
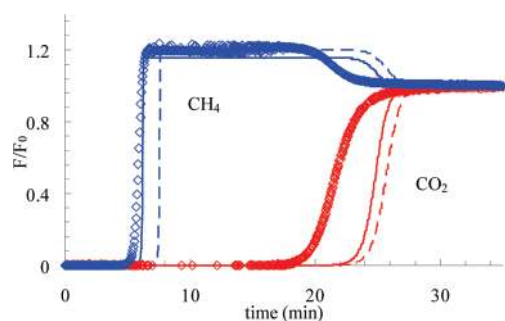
Figure 5. Breakthrough curves of the CO_2–CH_4 equimolar mixture at 303 K and 0.1 MPa on the Cu-BTC: experimental data (diamonds), simulated data based on pure component isotherms (dashed line), and simulated data based on coadsorption isotherms (full line).
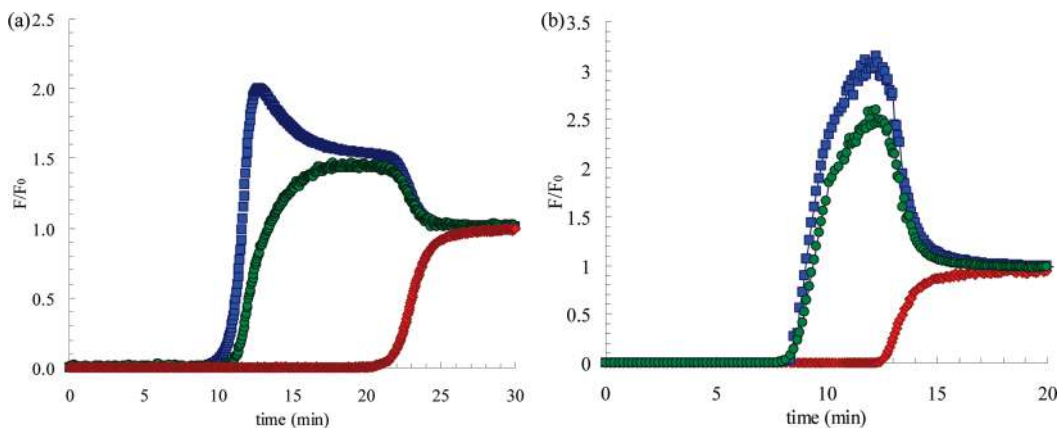
very sensibly on the isotherm parameters and on the order of magnitude of the diffusion coefficients. Since it is very difficult to reproduce the experimental isotherm with high precision, it follows that we cannot extract a reliable estimation of the diffusion coefficient from the breakthrough curve simulations.

Ternary Mixture Adsorption. Finally CO_2–CH_4–CO ternary experiments were carried out at 0.1 and 1.0 MPa (Figure 6). The breakthrough curves show that at 0.1 MPa CH_4 breaks through first, followed by CO. At 1.0 MPa CH_4 and CO break simultaneously through the column. Thus, at low pressure the CO_2–CH_4 selectivity is higher than the CO_2–CO selectivity, but at high pressures both values become equivalent. This corresponds to the observation that the pure component isotherms cross each other at ∼0.7 MPa (Figure 2). The higher affinity for CO at low pressure is most probably due to the direct interaction of CO with the Cu sites.

Since the ternary mixture CO_2–CH_4–CO represents a typical synthesis gas composition, we have used these data to calculate an empirical parameter that is a very important criterion for adsorbent selection: the delta loading or working capacity. The delta loading is defined as the difference of adsorbed amounts of one compound of the mixture between high pressure, i.e., at the pressure of the production step in the PSA process, and low pressure, i.e., at the pressure of the regeneration step in the process. The delta loading is therefore an indication of the adsorbent capacity in cyclic conditions. With our ternary mixture, the delta loading of CO_2 between 1.0 and 0.1 MPa is evaluated to be 7.37 mmol·g^{-1}. As an example, applying the IAST on previous published results,[51] the dynamic capacity of a BPL activated carbon is estimated to be 3.43 mmol·g^{-1} in the same conditions. For a Na–X,[52] the dynamic capacity is 1.44 mmol·g^{-1}. This comparison proves that Cu-BTC is a good adsorbent for CO_2 adsorption in synthesis gas mixtures.

Conclusions

Cu-BTC contains two types of pores, the large pores and the side pockets. GCMC simulation studies have shown that adsorption in the side pockets increases the CO_2–CH_4 selectivity of the material by 30 −50%.[53] The simulations predict a strong increase of the CO_2–CH_4 selectivity in the pressure range where the side pockets are filled, i.e., below ∼0.02 MPa.[18,19] Experimentally, we did not find a significant influence of the side pockets, neither on the selectivity at low pressure nor on the shape of the pure component isotherms. It seems as if the two types of pores had, after all, similar affinities for CO_2 and CH_4. The direct interaction with the accessible Cu sites in the large

Figure 6. Breakthrough curve of CO_2 (red), CH_4 (blue), and CO (green) at 0.1 (a) and 1.0 MPa (b) at 303 K for the 70−15−15 CO_2–CH_4–CO mixture.

pores holds the balance with the stronger confinement in the side pockets.

From an application point of view, Cu-BTC has very good selectivities and adsorption capacities with a measured CO_2 delta loading of the Cu-BTC of 7.37 mmol·g^{-1} between the production step at 1.0 MPa and the regeneration step at 0.1 MPa for the 70−15−15 CO_2−CH_4−CO separation. It makes it an attractive material for PSA applications. Its delta loading between 0.1 and 1.0 MPa is significantly higher than that of zeolite Na−X (delta loading of CO_2 in the same conditions of 1.44 mmol·g^{-1}) and of activated carbons (CO_2 delta loading of such an adsorbent is estimated to be 3.43 mmol·g^{-1}). Zeolite Na−X is highly selective but has an almost rectangular CO_2 isotherm. Saturation is reached at moderate pressure; thus, the difference of adsorption capacities between high pressure and low pressure is small. On the contrary, with an activated carbon as BPL, the shape of the pure CO_2 adsorption isotherm shows a moderate slope in the Henry region and the saturation is reached at very high pressure. Thus, the adsorbent chosen for PSA processes should ideally be a compromise between these two extremes: the curvature of the CO_2 adsorption isotherm should be similar to that of an activated carbon but attain saturation at the pressure of the production step of the PSA process. The Cu-BTC comes close to this good compromise. A second important criterion for adsorbent selection for a PSA with recovery of CO_2 is the selectivity of the adsorbent. Na−X is a highly CO_2-selective adsorbent, but the price to pay for the high selectivity is the difficult regeneration. Activated carbons are easily regenerable but not very selective (CO_2−CH_4 selectivity of 3.5).[37,51] Cu-BTC has an intermediate CO_2−CH_4 selectivity ranging from 4.8 to 11.5, which presents a significant gain compared to activated carbons.

Yet, before Cu-BTC can be used in separations on an industrial scale several remaining questions have to be resolved, in particular the issue of shaping of the material and its stability toward water vapor.[9,54]

Acknowledgment

Supporting Information Available: Text describing the experimental details of the breakthrough curves measurements and Cu-BTC characterization results, figures showing the breakthrough curve apparatus, powder XRD patterns, thermogravimetric analysis, nitrogen adsorption isotherms, breakthrough curves of CO_2−CH_4, and adsorption isotherms, and a table showing the input and isotherm parameters of the model. This information is available free of charge via the Internet at http://pubs.acs.org.

Notation

b_i = affinity coefficient in the Langmuir model (MPa^{-1})
B_i = affinity coefficient in the Langmuir model (m^3·mol^{-1})
C_i = concentration of component i in the gas phase (mol·m^{-3})
C_T = total concentration in the gas phase (mol·m^{-3})
D_L = axial dispersion coefficient (m^2·s^{-1})
D_c = diffusivity in the crystal (m^2·s^{-1})
k_t = film mass-transfer coefficient (m·s^{-1})
m_{ads} = mass of adsorbent (kg)
n_i = adsorbed phase concentration of component i (mol·m^{-3} of adsorbent)

n_i^* = adsorbed phase concentration in the equilibrium state of component i (mol·m^{-3})
p = pressure (bar)
Q = total volumetric gas flow rate (m^3·min^{-1})
q_i = adsorbed phase concentration of component i (mol·kg^{-1})
$q_{i,sat.}$, $n_{i,sat.}$ = maximum adsorbed amount of component i in the multisite Langmuir model
R_c = crystal radius (m)
r = radial coordinate (m)
t = time (s)
V_{col} = volume of the column (m^3)
v = interstitial velocity (m·s^{-1})
v_0 = interstitial velocity at the inlet of the column (m·s^{-1})
y_i = mole fraction of component i in the gas phase
z = axial coordinate (m)

Greek Letters

ε_i = interstitial porosity of the column
μ = first moment of the breakthrough curve (min)
ρ_{grain} = grain density of the adsorbent (kg·m^{-3})

Literature Cited

(1) Ferey, G. Hybrid Porous Solids: Past, Present, Future. *Chem. Soc. Rev.* **2008**, *37*, 191.

(2) Mueller, U.; Schubert, M.; Teich, F.; Puetter, H.; Schierle-Arndt, K.; Pastre, J. Metal-Organic Frameworks—Prospective Industrial Applications. *J. Mater. Chem.* **2006**, *16*, 626.

(3) Li, J. R.; Kuppler, R. J.; Zhou, H. C. Selective Gas Adsorption and Separation in Metal-Organic Frameworks. *Chem. Soc. Rev.* **2009**, *38*, 1477.

(4) Kuppler, R. J.; Timmons, D. J.; Fang, Q. R.; Li, J. R.; Makal, T. A.; Young, M. D.; Yuan, D.; Zhao, D.; Zhuang, W.; Zhou, H. C. Potential Applications of Metal-Organic Frameworks. *Coord. Chem. Rev.* **2009**, *253*, 3042.

(5) Bae, Y. S.; Farha, O. K.; Spokoyny, A. M.; Mirkin, C. A.; Hupp, J. T.; Snurr, R. Q. Carborane-Based Metal-Organic Frameworks as Highly Selective Sorbents for CO_2 over Methane. *Chem. Commun. (Cambridge, U.K.)* **2008**, *35*, 4135.

(6) Bae, Y. S.; Mulfort, K. L.; Frost, H.; Ryan, P.; Punnathanam, S.; Broadbelt, L. J.; Hupp, J. T.; Snurr, R. Q. Separation of CO_2 from CH_4 Using Mixed-Ligand Metal−Organic Frameworks. *Langmuir* **2008**, *24*, 8592.

(7) Chui, S. S. Y.; Lo, S. M. F.; Charmant, J. P. H.; Orpen, A. G.; Williams, I. D. A Chemically Functionalizable Nanoporous Material [Cu$_3$(TMA)$_2$(H$_2$O)$_3$]$_n$. *Science* **1999**, *283*, 1148.

(8) Wang, Q. M.; Shen, D. M.; Bulow, M.; Lau, M. L.; Deng, S. G.; Fitch, F. R.; Lemcoff, N. O.; Semanscin, J. Metallo-Organic Molecular Sieve for Gas Separation and Purification. *Microporous Mesoporous Mater.* **2002**, *55*, 217.

(9) Liang, Z. J.; Marshall, M.; Chaffee, A. L. CO_2 Adsorption-Based Separation by Metal Organic Framework (Cu-BTC) versus Zeolite (13X). *Energy Fuels* **2009**, *23*, 2785.

(10) Garcia-Perez, E.; Gascon, J.; Morales-Florez, V.; Castillo, J. M.; Kapteijn, F.; Calero, S. Identification of Adsorption Sites in Cu-BTC by Experimentation and Molecular Simulation. *Langmuir* **2009**, *25*, 1725.

(11) Millward, A. R.; Yaghi, O. M. Metal−Organic Frameworks with Exceptionally High Capacity for Storage of Carbon Dioxide at Room Temperature. *J. Am. Chem. Soc.* **2005**, *127*, 17998.

(12) Farrusseng, D.; Daniel, C.; Gaudillere, C.; Ravon, U.; Schuurman, Y.; Mirodatos, C.; Dubbeldam, D.; Frost, H.; Snurr, R. Q. Heats of Adsorption for Seven Gases in Three Metal−Organic Frameworks: Systematic Comparison of Experiment and Simulation. *Langmuir* **2009**, *25*, 7383.

(13) Yazaydin, A. O.; Benin, A. I.; Faheem, S. A.; Jakubczak, P.; Low, J. J.; Willis, R. R.; Snurr, R. Q. Enhanced CO_2 Adsorption in Metal−Organic Frameworks via Occupation of Open Metal Sites by Coordinated Water Molecules. *Chem. Mater.* **2009**, *21*, 1425.

(14) Cavenati, S.; Grande, C. A.; Rodrigues, A. E. Metal Organic Framework Adsorbent for Biogas Upgrading. *Ind. Eng. Chem. Res.* **2008**, *47*, 6333.

(15) Senkovska, I.; Kaskel, S. High Pressure Methane Adsorption in the Metal-Organic Frameworks Cu$_3$(btc)$_2$, Zn$_2$(bdc)$_2$dabco, and Cr$_3$F-(H2O)$_2$O(bdc)$_3$. *Microporous Mesoporous Mater.* **2008**, *112*, 108.

(16) Chowdhury, P.; Bikkina, C.; Meister, D.; Dreisbach, F.; Gumma, S. Comparison of Adsorption Isotherms on Cu-BTC Metal Organic Frameworks Synthesized from Different Routes. *Microporous Mesoporous Mater.* **2009**, *117*, 406.

(17) Cheng, Y.; Kondo, A.; Noguchi, H.; Kajiro, H.; Urita, K.; Ohba, T.; Kaneko, K.; Kanoh, H. Reversible Structural Change of Cu-MOF on Exposure to Water and its CO_2 Adsorptivity. *Langmuir* **2009**, *25*, 4510.

(18) Babarao, R.; Jiang, J. W.; Sandler, S. I. Molecular Simulations for Adsorptive Separation of CO_2/CH_4 Mixture in Metal-Exposed, Catenated, and Charged Metal−Organic Frameworks. *Langmuir* **2009**, *25*, 5239.

(19) Yang, Q. Y.; Zhong, C. L. Molecular Simulation of Carbon Dioxide/Methane/Hydrogen Mixture Adsorption in Metal−Organic Frameworks. *J. Phys. Chem. B* **2006**, *110*, 17776.

(20) Martin-Calvo, A.; Garcia-Perez, E.; Castillo, J. M.; Calero, S. Molecular Simulations for Adsorption and Separation of Natural Gas in IRMOF-1 and Cu-BTC Metal-Organic Frameworks. *Phys. Chem. Chem. Phys.* **2008**, *10*, 7085.

(21) Krishna, R. Describing the Diffusion of Guest Molecules Inside Porous Structures. *J. Phys. Chem. C* **2009**, *113*, 19756.

(22) Keskin, S.; Liu, J. C.; Johnson, J. K.; Sholl, D. S. Atomically Detailed Models of Gas Mixture Diffusion through CuBTC Membranes. *Microporous Mesoporous Mater.* **2009**, *125*, 101.

(23) Bordiga, S.; Regli, L.; Bonino, F.; Groppo, E.; Lamberti, C.; Xiao, B.; Wheatley, P. S.; Morris, R. E.; Zecchina, A. Adsorption Properties of HKUST-1 toward Hydrogen and Other Small Molecules Monitored by IR. *Phys. Chem. Chem. Phys.* **2007**, *9*, 2676.

(24) Dreisbach, F.; Seif, A. H. R.; Losch, H. W. Measuring Techniques for Gas-Phase Adsorption Equilibria. *Chem. Ing. Tech.* **2002**, *74*, 1353.

(25) De Weireld, G.; Frere, M.; Jadot, R. Automated Determination of High-Temperature and High-Pressure Gas Adsorption Isotherms Using a Magnetic Suspension Balance. *Meas. Sci. Technol.* **1999**, *10*, 117.

(26) Rouquerol, F.; Rouquerol, J.; Sing, K. S. W. *Adsorption by Powders and Porous Solids*; Academic Press: London, San Diego, 1999.

(27) Span, R.; Wagner, W. A New Equation of State for Carbon Dioxide Covering the Fluid Region from the Triple-Point Temperature to 1100 K at Pressures up to 800 MPa. *J. Phys. Chem. Ref. Data* **1996**, *25*, 1509.

(28) Setzmann, U.; Wagner, W. A New Equation of State and Tables of Thermodynamic Properties for Methane Covering the Range from the Melting Point to 625 K at Pressures up to 1000 MPa. *J. Phys. Chem. Ref. Data* **1991**, *20*, 1061.

(29) McCarty, R. D.; Arps, V. D. A New Wide Range Equation of State for Helium. *Advances in Cryogenic Engineering* **1990**, *35*, 1465.

(30) Vishnyakov, A.; Ravikovitch, P. I.; Neimark, A. V.; Bulow, M.; Wang, Q. M. Nanopore Structure and Sorption Properties of Cu-BTC Metal−Organic Framework. *Nano Lett.* **2003**, *3*, 713.

(31) Krungleviciute, V.; Lask, K.; Heroux, L.; Migone, A. D.; Lee, J. Y.; Li, J.; Skoulidas, A. Argon Adsorption on Cu$_3$(Benzene-1,3,5-tricarboxylate)$_2$(H$_2$O)$_3$ Metal−Organic Framework. *Langmuir* **2007**, *23*, 3106.

(32) Krawiec, P.; Kramer, M.; Sabo, M.; Kunschke, R.; Frode, H.; Kaskel, S. Improved Hydrogen Storage in the Metal-Organic Framework Cu$_3$(BTC)$_2$. *Adv. Eng. Mater.* **2006**, *8*, 293.

(33) Walton, K. S.; Snurr, R. Q. Applicability of the BET Method for Determining Surface Areas of Microporous Metal−Organic Frameworks. *J. Am. Chem. Soc.* **2007**, *129*, 8552.

(34) Sing, K. S. W.; Everett, D. H.; Haul, R. A. W.; Moscou, L.; Pierotti, R. A.; Rouquerol, J.; Siemieniewska, T. Reporting Physisorption Data for Gas/Solid Systems with Special Reference to the Determination of Surface Area and Porosity. *Pure Appl. Chem.* **1985**, *57*, 603.

(35) Hartmann, M.; Kunz, S.; Himsl, D.; Tangermann, O.; Ernst, S.; Wagener, A. Adsorptive Separation of Isobutene and Isobutane on Cu$_3$(BTC)$_2$. *Langmuir* **2008**, *24*, 8634.

(36) Ghoufi, A.; Gaberova, L.; Rouquerol, J.; Vincent, D.; Llewellyn, P. L.; Maurin, G. Adsorption of CO_2, CH_4 and Their Binary Mixture in Faujasite NaY: A Combination of Molecular Simulations with Gravimetry-Manometry and Microcalorimetry Measurements. *Microporous Mesoporous Mater.* **2009**, *119*, 117.

(37) Ritter, J. A.; Yang, R. T. Equilibrium Adsorption of Multicomponent Gas-Mixtures at Elevated Pressures. *Ind. Eng. Chem. Res.* **1987**, *26*, 1679.

(38) Myers, A.; Prausnitz, J. Thermodynamics of Mixed-Gas Adsorption. *AIChE J.* **1965**, *11*, 121.

(39) Ruthven, D. M. *Principles of Adsorption and Adsorption Processes*; Wiley-Interscience: New York, 1984.

(40) Saha, D.; Deng, S. G. Adsorption Equilibria and Kinetics of Carbon Monoxide on Zeolite 5A, 13X, MOF-5, and MOF-177. *J. Chem. Eng. Data* **2009**, *54*, 2245.

(41) Zhao, Z. X.; Li, Z.; Lin, Y. S. Adsorption and Diffusion of Carbon Dioxide on Metal−Organic Framework (MOF-5). *Ind. Eng. Chem. Res.* **2009**, *48*, 10015.

(42) Salles, F.; Jobic, H.; Devic, T.; Llewellyn, P. L.; Serre, C.; Ferey, G.; Maurin, G. Self and Transport Diffusivity of CO_2 in the Metal−Organic Framework MIL-47(V) Explored by Quasi-Elastic Neutron Scattering Experiments and Molecular Dynamics Simulations. *ACS Nano* **2010**, *4*, 143.

(43) Ma, Y. H.; Mancel, C. Diffusion Studies of CO_2, NO, NO_2, and SO_2 on Molecular Sieve Zeolites by Gas Chromatography. *AIChE J.* **2010**, *18*, 1148.

(44) Onyestyak, G.; Rees, L. V. C. Frequency Response Study of Adsorbate Mobilities of Different Character in Various Commercial Adsorbents. *J. Phys. Chem. B* **1999**, *103*, 7469.

(45) Grenier, Ph.; Malka-Edery, A.; Bourdin, V. A Temperature Frequency Response Method for Adsorption Kinetics Measurements. *Adsorption* **1999**, *5*, 135.

(46) Bulow, M. Complex Sorption Kinetics of Carbon Dioxide in NaX-Zeolite Crystals. *Adsorption* **2002**, *8*, 9.

(47) Goubaru, A.; Abe, S.; Ermalina, K. K. Inverse Analyses of Diffusion Processes in Type 13X zeolite particles. *Appl. Energy* **2005**, *81*, 277.

(48) Kamiuto, K.; Goubaru, A.; Ermalina, K. K. Diffusion Coefficients of Carbon Dioxide within Type 13X Zeolite Particles. *Chem. Eng. Commun.* **2006**, *193*, 628.

(49) Plant, D.; Jobic, H.; Llewellyn, P.; Maurin, G. Diffusion of CO_2 in NaY and NaX Faujasite Systems: Quasi-Elastic Neutron Scattering Experiments and Molecular Dynamics Simulations. *Eur. Phys. J.−Spec. Top.* **2007**, *141*, 127.

(50) Kärger, J.; Ruthven, D. M. *Diffusion in Zeolites and Other Microporous Solids*; Wiley-Interscience: New York, 1992.

(51) Wilson, R. J.; Danner, R. P. Adsorption of Synthesis Gas-Mixture Components on Activated Carbon. *J. Chem. Eng. Data* **1983**, *28*, 14.

(52) Belmabkhout, Y.; Pirngruber, G. D.; Jolimaitre, E.; Methivier, A. A Complete Experimental Approach for Synthesis Gas Separation Studies Using Static Gravimetric and Column Breakthrough Experiments. *Adsorption* **2007**, *13*, 341.

(53) Xue, C. Y.; Yang, Q. Y.; Zhong, C. L. Effects of the Side Pockets on Gas Separation in Metal-Organic Framework Cu-BTC: A Molecular Simulation Study. *Mol. Simul.* **2009**, *35*, 1249.

(54) Schlichte, K.; Kratzke, T.; Kaskel, S. Improved Synthesis, Thermal Stability and Catalytic Properties of the Metal-Organic Framework Compound Cu$_3$(BTC)$_2$. *Microporous Mesoporous Mater.* **2004**, *73*, 81.